



*Journal of Geophysical Research: Planets*

Supporting Information for

**Surface Energy Budget, Albedo and Thermal Inertia at Jezero Crater, Mars, as observed from the Mars 2020 MEDA instrument**

G. M. Martínez<sup>1,2</sup>, E. Sebastián<sup>3</sup>, A. Vicente-Retortillo<sup>3,2</sup>, M. D. Smith<sup>4</sup>, J. R. Johnson<sup>5</sup>, E. Fischer<sup>2</sup>, H. Savijärvi<sup>6</sup>, D. Toledo<sup>7</sup>, R. Hueso<sup>8</sup>, L. Mora-Sotomayor<sup>3</sup>, H. Gillespie<sup>1</sup>, A. Munguira<sup>8</sup>, A. Sánchez-Lavega<sup>8</sup>, M. T. Lemmon<sup>9</sup>, F. Gómez<sup>3</sup>, J. Polkko<sup>10</sup>, L. Mandon<sup>11</sup>, V. Apéstigue<sup>6</sup>, I. Arruego<sup>6</sup>, M. Ramos<sup>12</sup>, P. Conrad<sup>13</sup>, C. E. Newman<sup>14</sup>, M. Torre Juarez<sup>15</sup>, F. Jordan<sup>3</sup>, L. K. Tamppari<sup>15</sup>, T. H. McConnochie<sup>9</sup>, A.-M. Harri<sup>10</sup>, M. Genzer<sup>10</sup>, M. Hieta<sup>10</sup>, M.-P. Zorzano<sup>3</sup>, M. Siegler<sup>16</sup>, O. Prieto<sup>3</sup>, A. Molina<sup>3</sup>, and J. A. Rodríguez-Manfredi<sup>3</sup>

<sup>1</sup>Lunar and Planetary Institute, Universities Space Research Association, Houston, TX, USA.

<sup>2</sup>University of Michigan, USA

<sup>3</sup>Centro de Astrobiología (INTA-CSIC), Spain

<sup>4</sup>NASA Goddard Space Flight Center, USA

<sup>5</sup>John Hopkins University/APL, USA

<sup>6</sup>University of Helsinki, Finland

<sup>7</sup>Instituto Nacional de Técnica Aeroespacial, Spain

<sup>8</sup> Universidad del País Vasco/Euskal Herriko Unibertsitatea, Spain

<sup>9</sup>Space Science Institute, USA

<sup>10</sup>Finnish Meteorological Institute, Finland

<sup>11</sup>Laboratoire d'Etudes Spatiales et d'Instrumentation en Astrophysique, Observatoire de Paris-PSL, France

<sup>12</sup>Universidad de Alcalá de Henares, Spain

<sup>13</sup>Carnegie Institution for Science, USA

<sup>14</sup>Aeolis Research, USA

<sup>15</sup>Jet Propulsion Laboratory, California Institute of Technology, USA

<sup>16</sup>Planetary Science Institute, USA

## **Contents of this file**

Figures S1 to S10.

## **Additional Supporting Information (Files uploaded separately)**

Captions for ds01 to ds03.

## **Introduction**

The supporting information for this manuscript includes ten figures (Figs. S1 to S10, shown below) and three datasets uploaded separately but with an explanation of their contents given at the end of this document.

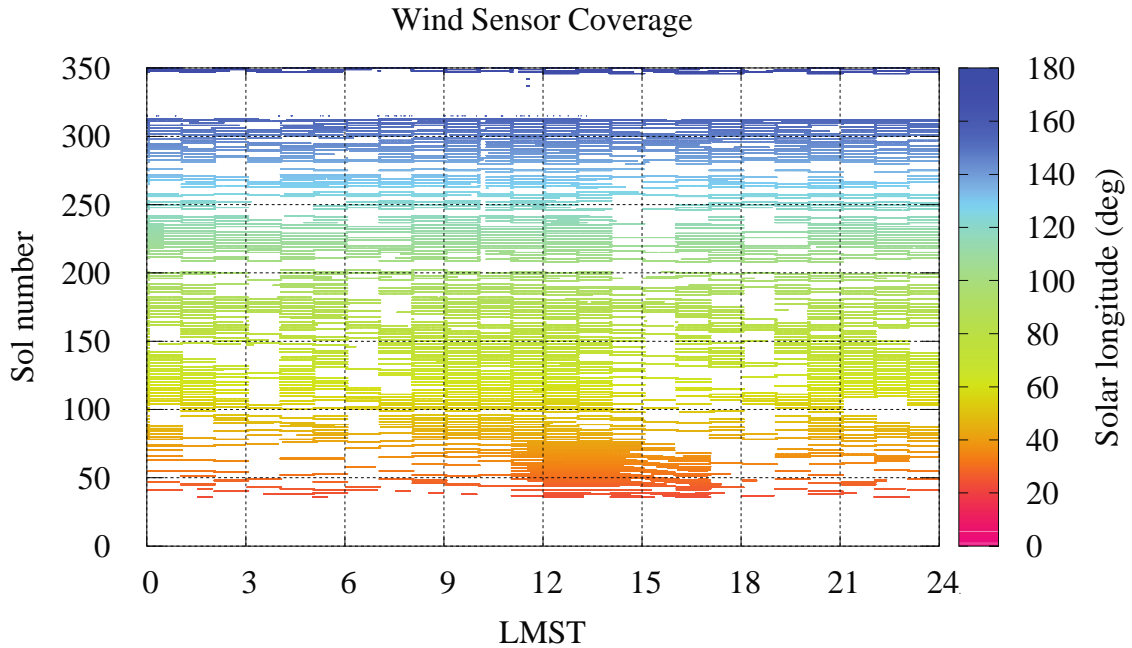


**Figure S1.** Temporal coverage of the MEDA WS during the first 350 sols of the M2020 mission. The WS was damaged by the regional dust storm occurred around sols 312–318 ( $L_s$  152°–156°), which led the team to turn it off for assessment. After identification of the WS components that were damaged and that hindered its performance, the WS resumed activity on sol 346. At the time of this writing, the MEDA team is working on retrieving reliable wind speed measurements and directions for sols  $> 346$ .

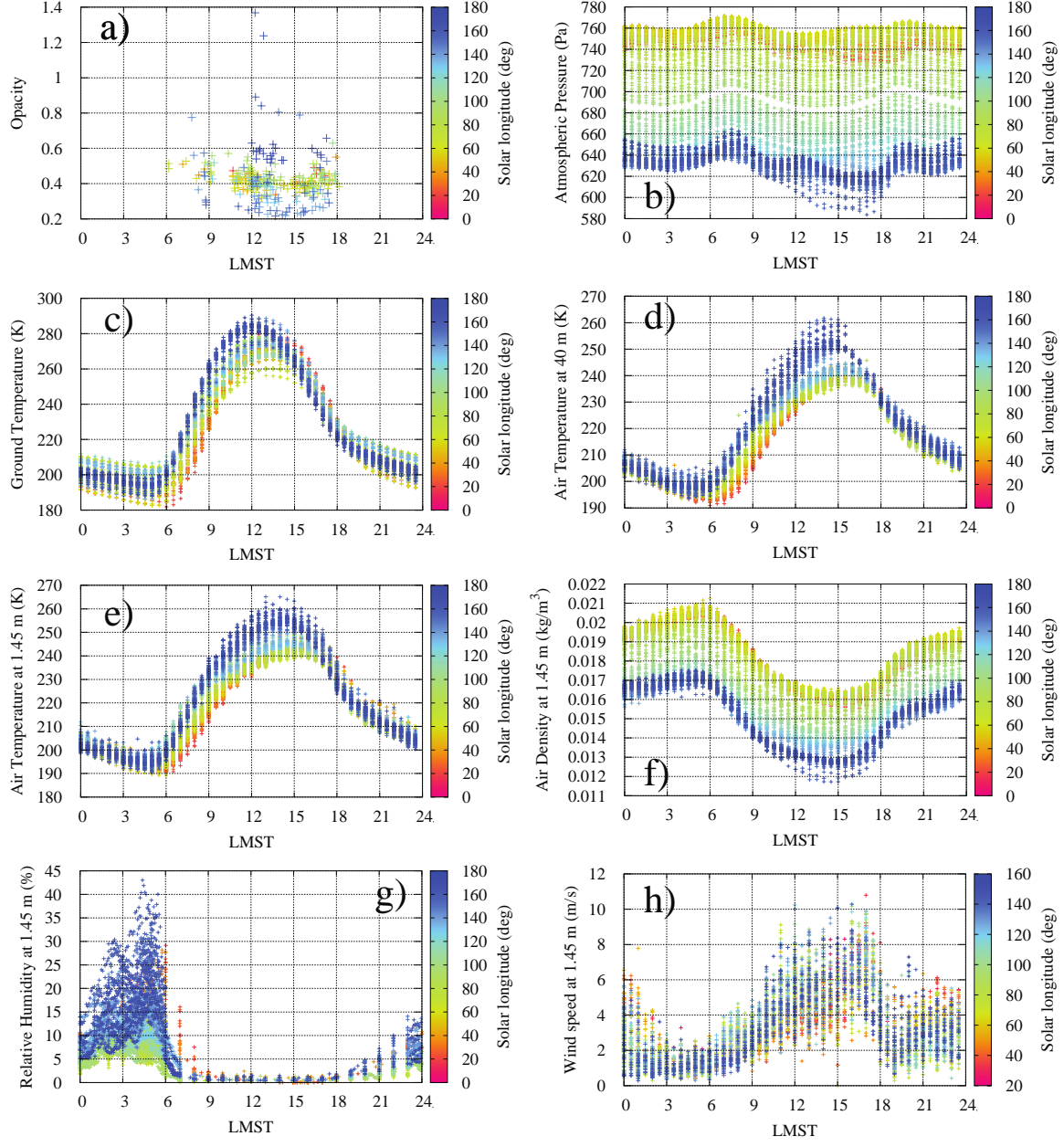


**Figure S2.** Diurnal evolution of the environmental quantities measured by Mastcam-Z and MEDA during the first 350 sols of the M2020 mission. **(a)** Aerosol opacity at 0.88  $\mu\text{m}$  retrieved by the Mastcam-Z instrument. **(b)** Atmospheric pressure. **(c)** Ground temperature. **(d)** Air temperature at about 40 m. **(e)** Air temperature at 1.45 m, where only ATS1, ATS2, and ATS3 have been considered. **(f)** Atmospheric density at 1.45 m. **(g)** Relative humidity at 1.5 m. **(h)** Nighttime maximum water vapor VMR.

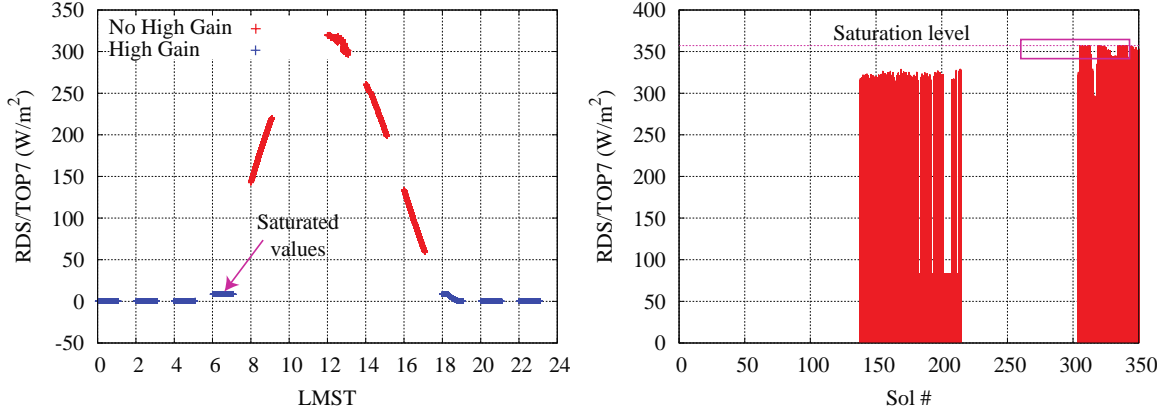


**Figure S3.** The two scenarios under which RDS/TOP7 measurements are saturated. (**Left**) RDS/TOP7 CAL measurements on sol 130 as a function of LMST. This is an example of saturated values when the RDS operated in “high gain” mode during sunrise hours, which resulted in saturated values  $\sim 8.5 \text{ W/m}^2$  (pink arrow). (**Right**) Daily maximum RDS/TOP7 CAL values, typically achieved near noon, as a function of sol number. In the vicinity of noon beyond sol  $\sim 270$  ( $L_s \sim 131^\circ$ ; pink rectangle), the incident solar flux was higher than the upper bound of the range established in pre-flight calibrations on Earth ( $\sim 356 \text{ W/m}^2$ ; dashed pink line).

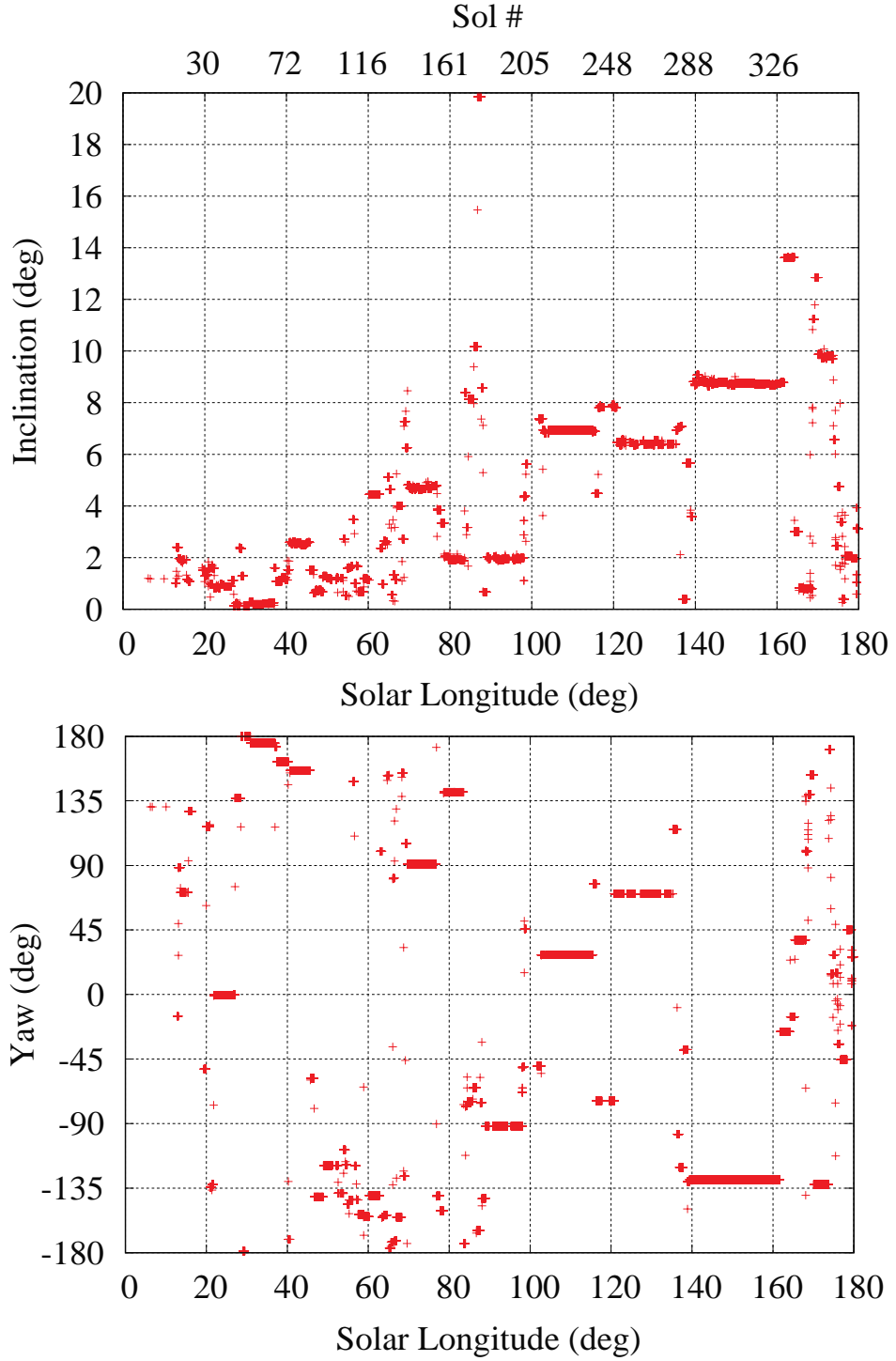


**Figure S4.** (Top) Inclination of the terrain traversed by the Curiosity rover as a function of Ls and Sol #. It is calculated as  $\sqrt{(roll^2 + pitch^2)}$ , where values of the rover roll and pitch are available in the PDS as ‘Ancillary Data’ (\*DER\_ANCILLARY\* files).  
**(Bottom).** Rover yaw, defined as the counterclockwise rotation angle about the +Z-axis of the M2020 local level frame.

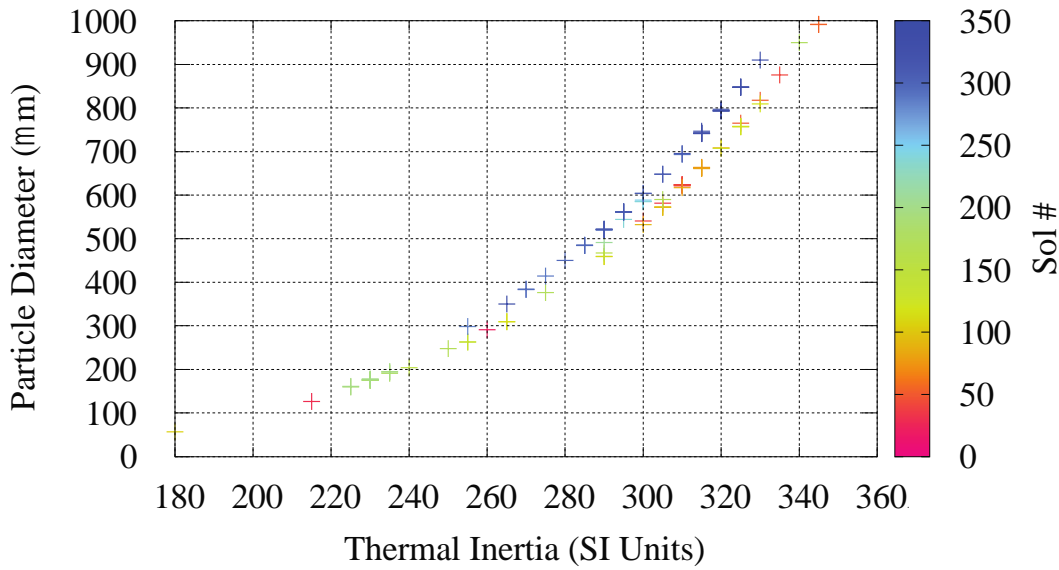


**Figure S5.** Particle size as a function of thermal inertia derived from MEDA for the first 350 sols (color-coded) of the M2020 mission. These values have been estimated using an experimentally-derived relationship between thermal inertia, soil density and specific heat, and atmospheric pressure (Presley and Christensen, 1997), which is only applicable to  $TI$  values  $< 350$  SI units and that has an uncertainty  $< 15\%$ .

### Jezero Crater, 18.36N

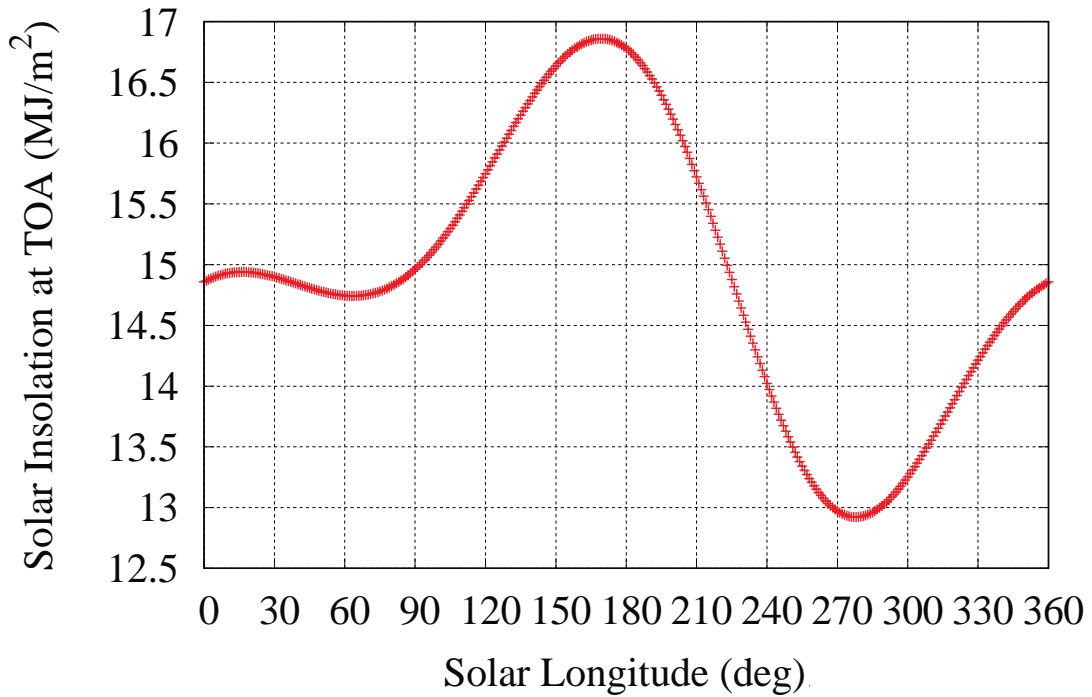


**Figure S6.** Solar insolation (defined as the solar irradiance integrated over one sol) at the top of the atmosphere (TOA) at the latitude of the Mars 2020 landing site, simulated with COMIMART (Vicente-Retortillo et al., 2015). Over the first 350 sols of the Mars 2020 mission ( $L_s \sim 6^\circ$ – $174^\circ$ ), it shows a relative minimum at  $L_s \sim 65^\circ$  and an absolute maximum at  $L_s \sim 170^\circ$ .

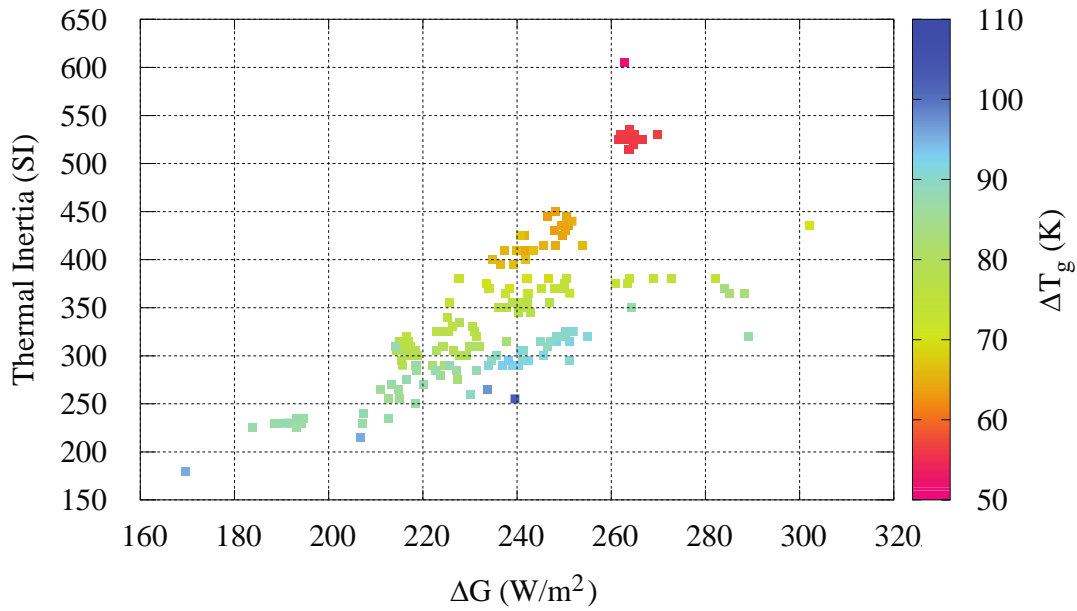


**Figure S7.** Thermal inertia as a function of the diurnal amplitude of the net heat flux,  $\Delta G$  (difference between the daily maximum and minimum), with color bar representing the diurnal amplitude of the ground temperature,  $\Delta T_g$ . Higher  $TI$  values typically correspond with larger  $\Delta G$  and lower  $\Delta T_g$ .

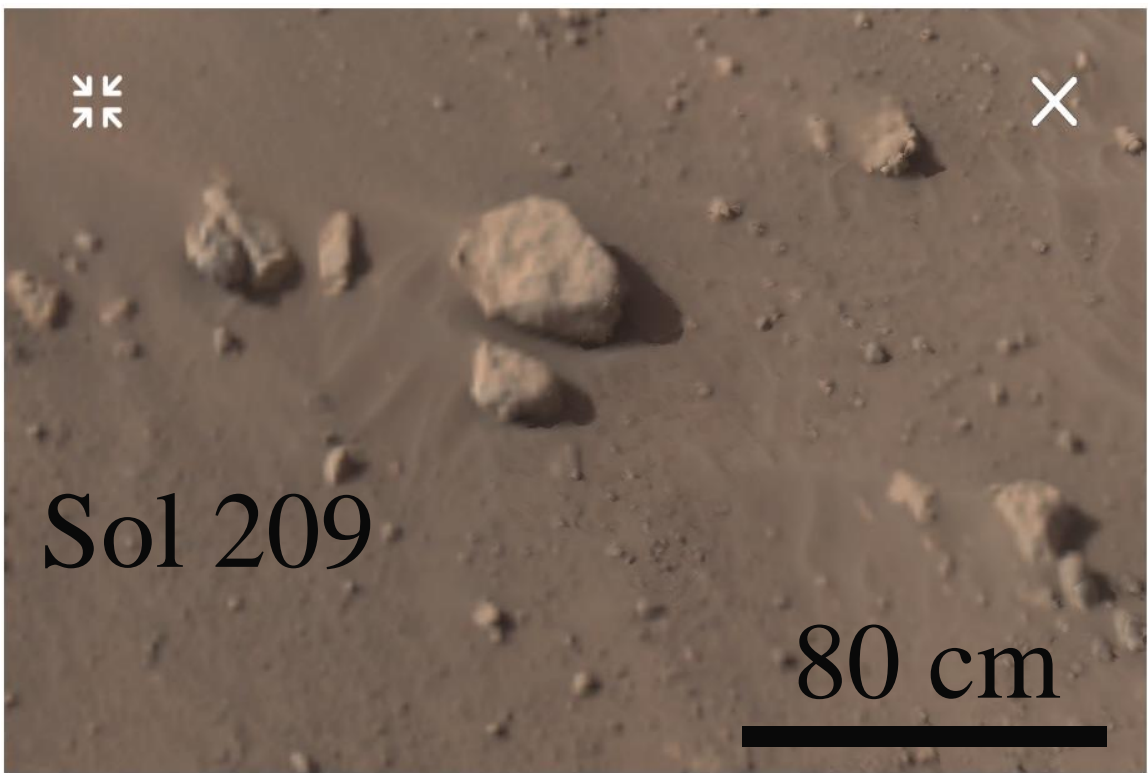
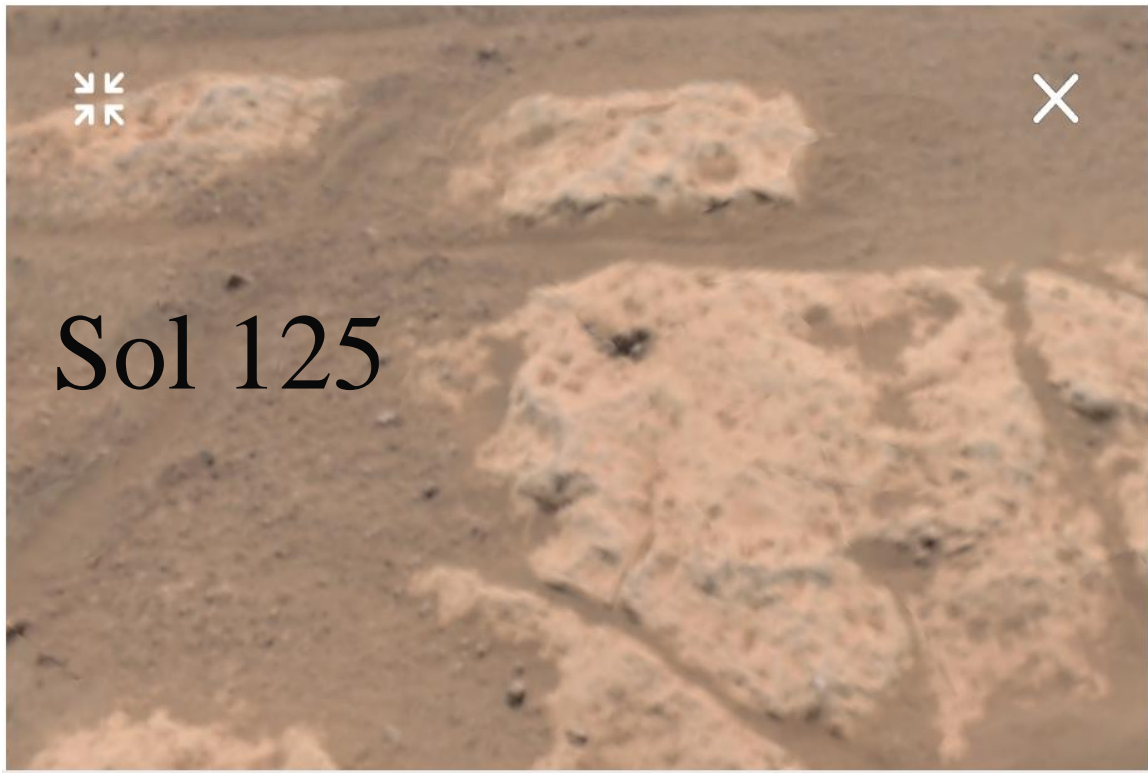


**Figure S8.** FoV of TIRS downward-looking channels on sols 125 (top) and 209 (bottom), corresponding to the terrains with the highest and lowest near-noon albedo values.

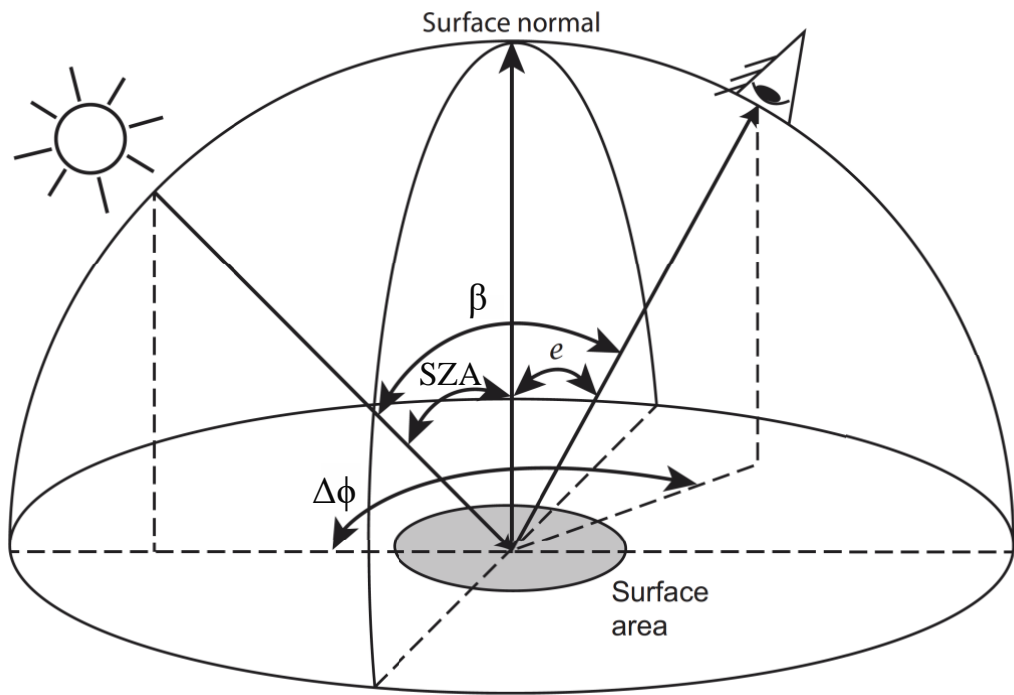


**Figure S9.** Illustration of illumination and observing angles. SZA represents the solar zenith angle,  $e$  the emission angle corresponding to the TIRS/IR3 channel, and  $\Delta\phi = |\phi_s - \phi_{TIRS}| + 180^\circ$  is the absolute difference between the solar azimuth angle and TIRS' azimuth angle. Adapted from Shepard (2017).

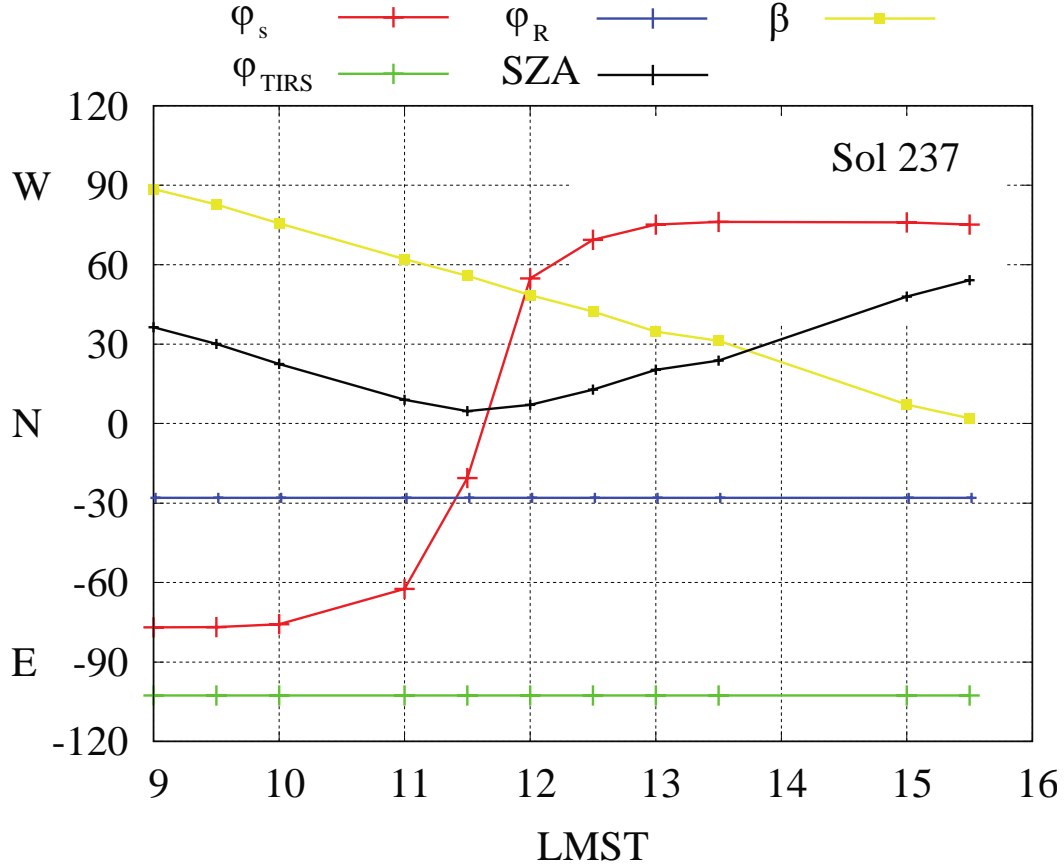


**Figure S10.** Illumination and viewing geometry on sol 237 as a function of LMST. On this sol the rover's yaw was  $\phi_R = -27^\circ$  (blue), which resulted in  $\phi_{TIRS} = -102^\circ$  (green). Therefore, the TIRS' FoV was pointing approximately towards East. Under this geometry, the Sun was directly behind TIRS' FoV at 15:30 LMST, when the phase angle  $\beta$  (golden) approached  $0^\circ$  and the solar zenith angle SZA  $\sim 54^\circ$  (black).

**Data Set S1.** Angular correction factor as a function of aerosol opacity and solar zenith angle (SZA).

**Data Set S2.** Conversion factor from 0.19–1.2 (RDS/TOP7) to 0.19–5  $\mu\text{m}$  ( $SW_d$ ) as a function of aerosol opacity.

**Data Set S3.** List of sols and LMST corresponding to TIRS in-flight calibrations.

**References:**

Shepard, M. K. (2017). *Introduction to planetary photometry*. Cambridge University Press.